Supporting Information for:

Linkage Between Proximal and Distal Movements of P450cam Induced by Putidaredoxin

Shu-Hao Liou[1,2‡], Shih-Wei Chuo[1‡], Yudong Qiu[1], Lee-Ping Wang[1] and David B. Goodin[1*]

[1]Department of Chemistry, University of California, Davis, One Shields Avenue, Davis, California 95616, USA

[2]Gruss-Lipper Biophotonics Center, Department of Anatomy and Structural Biology, Albert Einstein College of Medicine, Bronx, NY 10461, USA

Protein	Label	Predicted Mass	Actual Mass
BSL-AC	-	46426	46420
	BSL	46890	46880
BSL-CD	-	46409	46407
	BSL	46873	46877
BSL-AJ	-	46369	46364
	BSL	46833	46836
W106A Pdx	-	11304	11303
D38A Pdx	-	11375	11374

Table S1: The mass of the proteins with and without label.

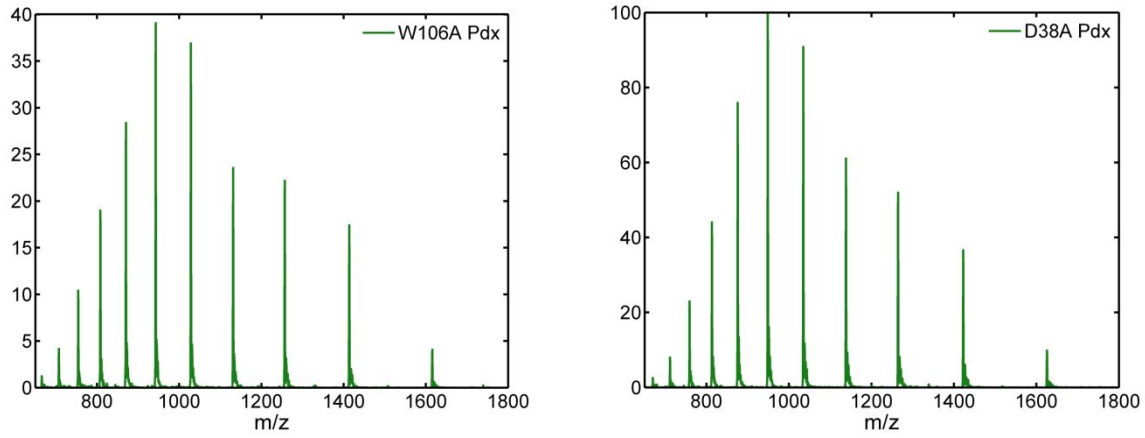

Figure S1: The ESI-MS spectra of Pdx mutants, W106A (left) and D38A (right).

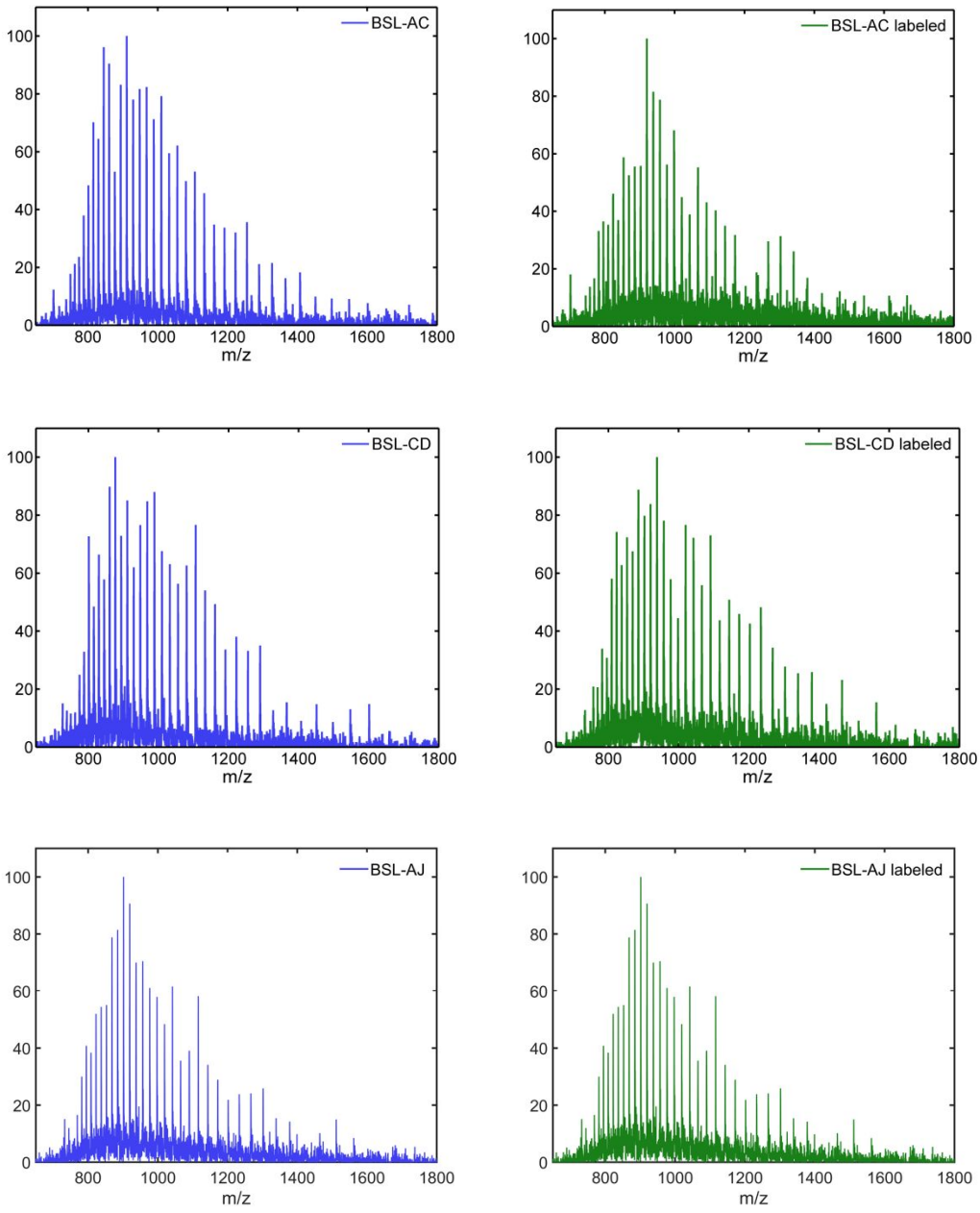

Figure S2: The ESI-MS spectra of BSL-AC, BSL-CD and BSL-AJ P450cam without (blue) or with BSL attachment (green), respectively.

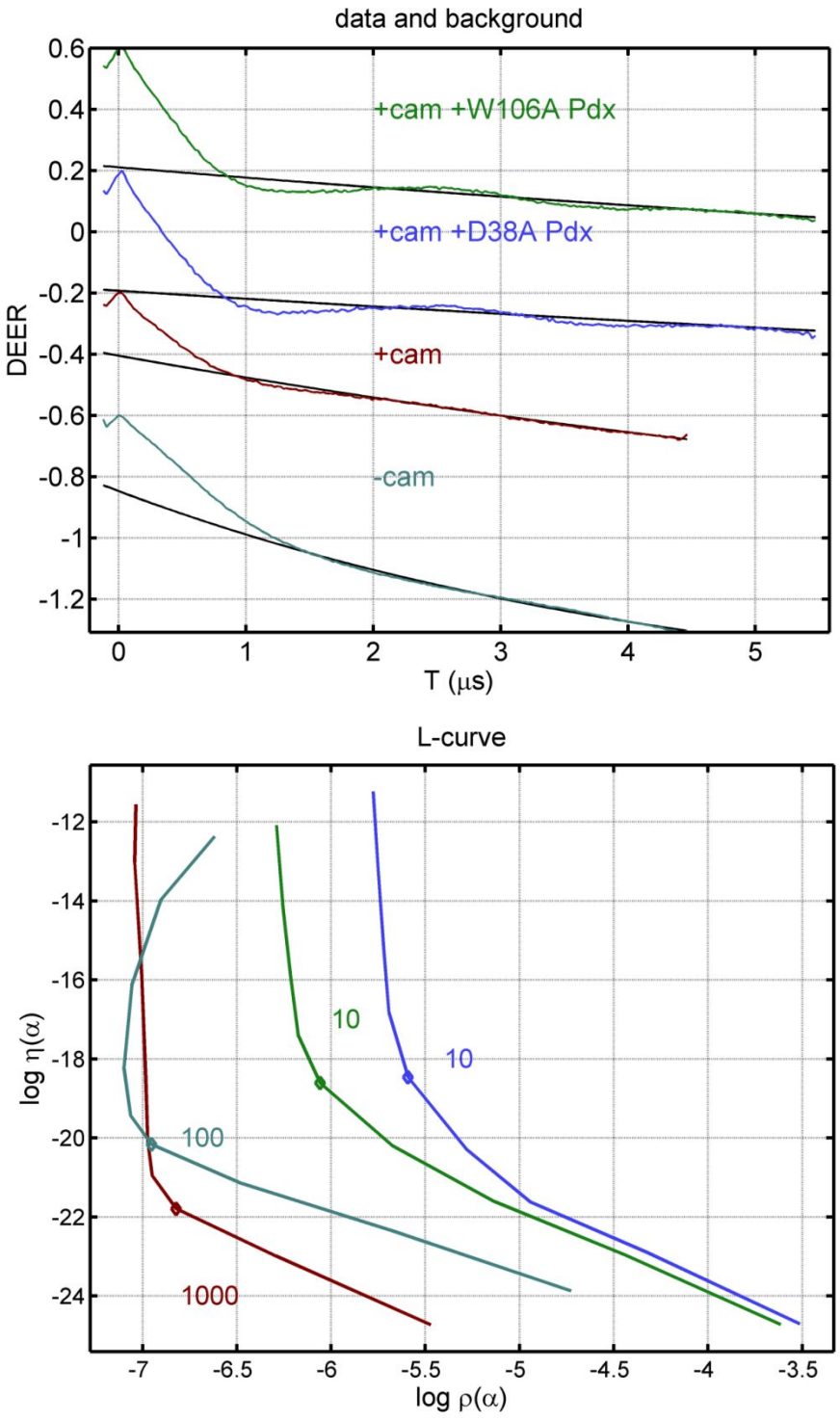

Figure S3: Background subtractions and L-curves for the DEER data in Figure 3. The numbers shown in the L-curve figure are the regularization parameters.

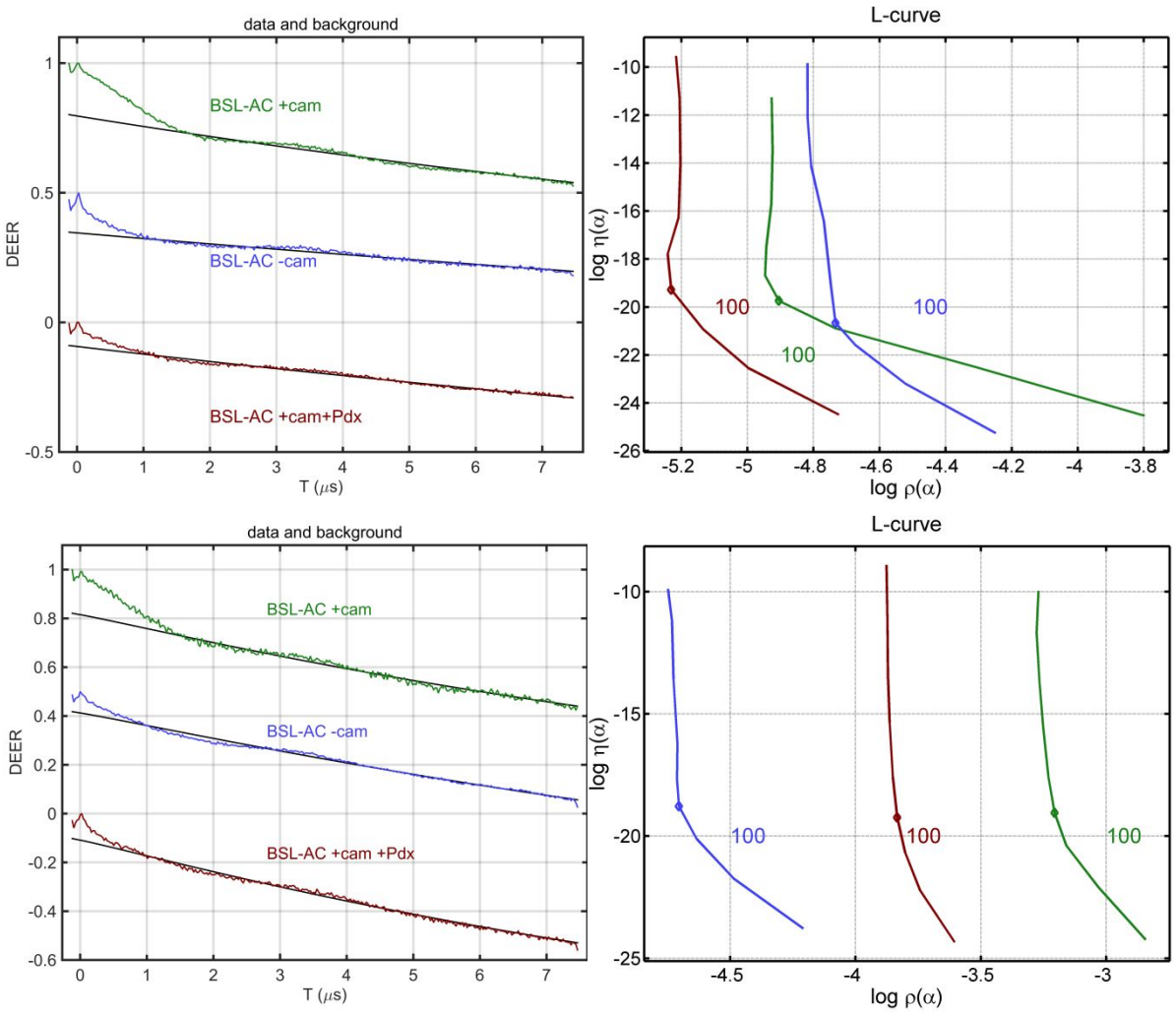

Figure S4: Background subtractions (left) and L-curves (right) for the BSL-AC DEER data from two protein batches.

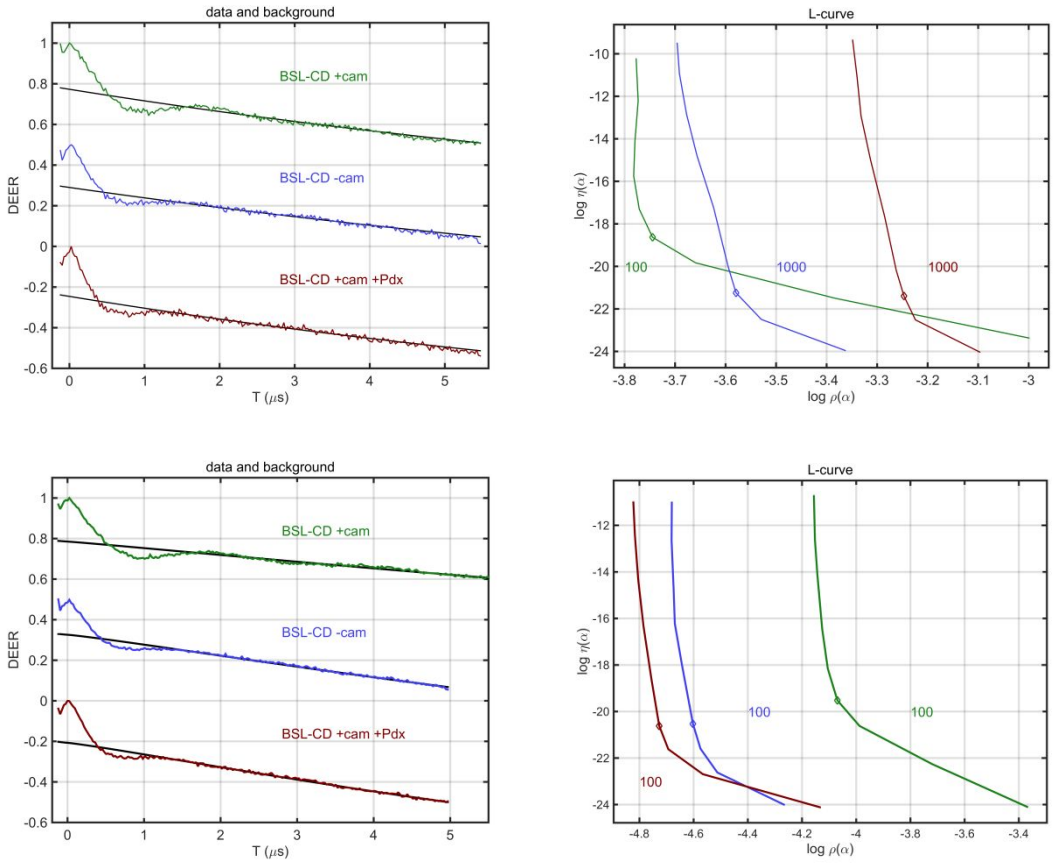

Figure S5: Background subtractions (left) and L-curves (right) of the BSL-CD DEER data from two protein batches.

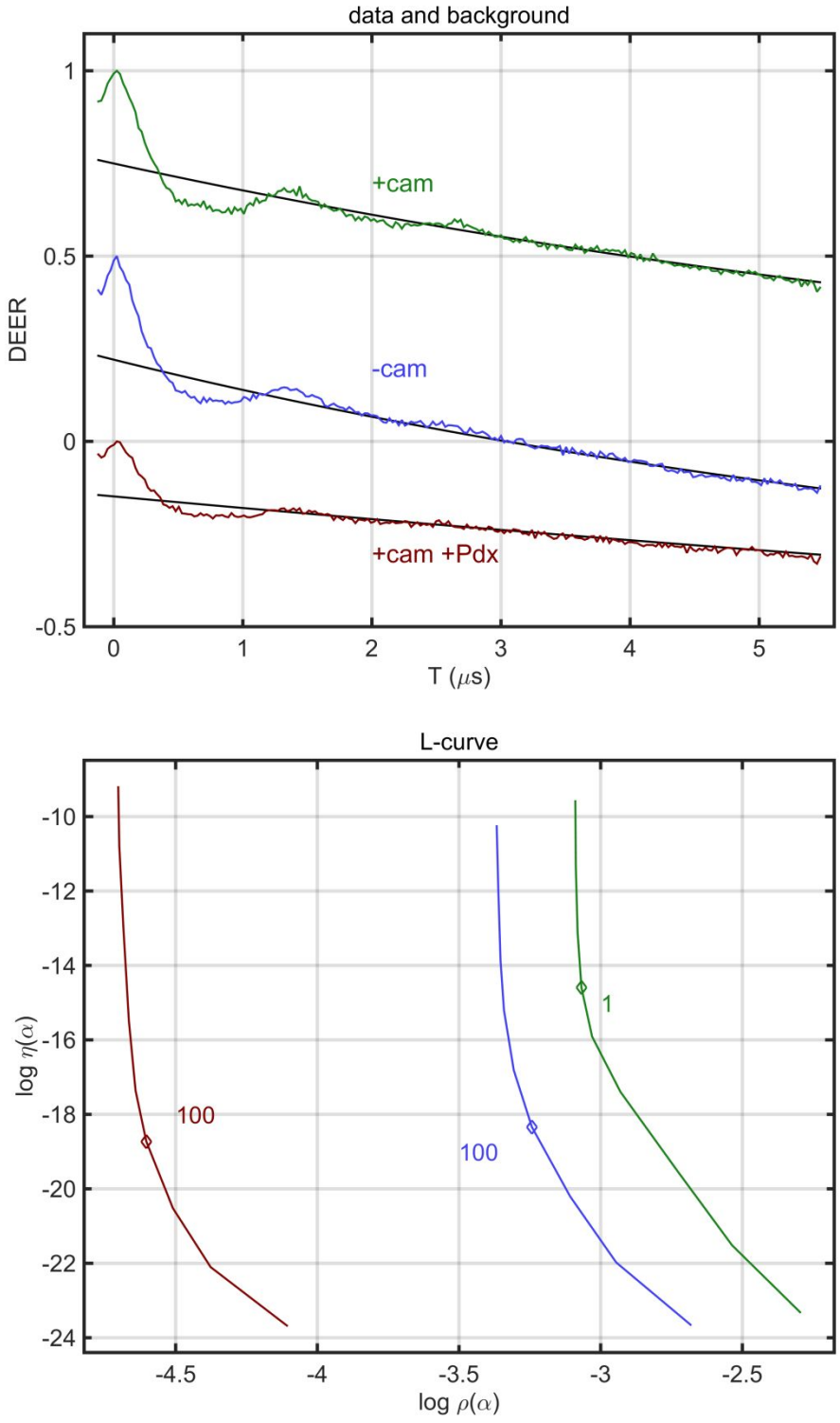

Figure S6. Background subtractions (top) and L-curves (bottom) of BSL-AJ DEER data.

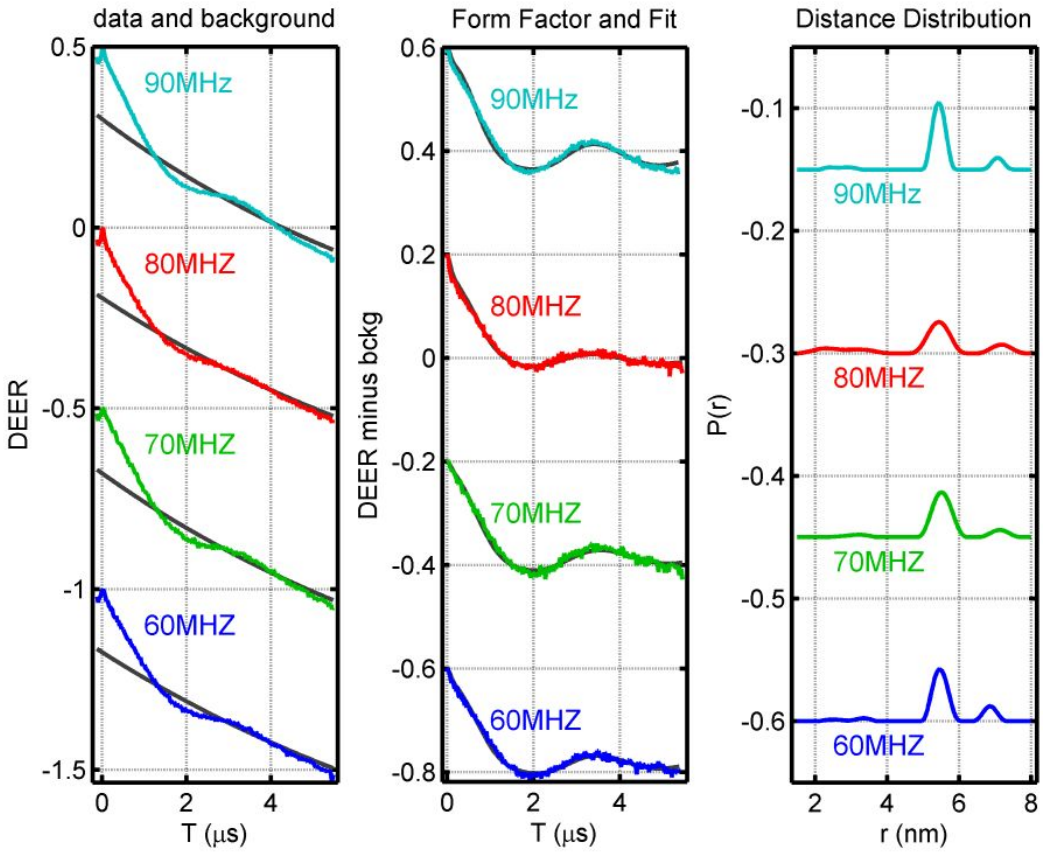

Figure S7: A series of orientation selection experiments for camphor-bound BSL-AC at different intervals (90, 80, 70 and 60 MHz) of the probe and pump frequency.

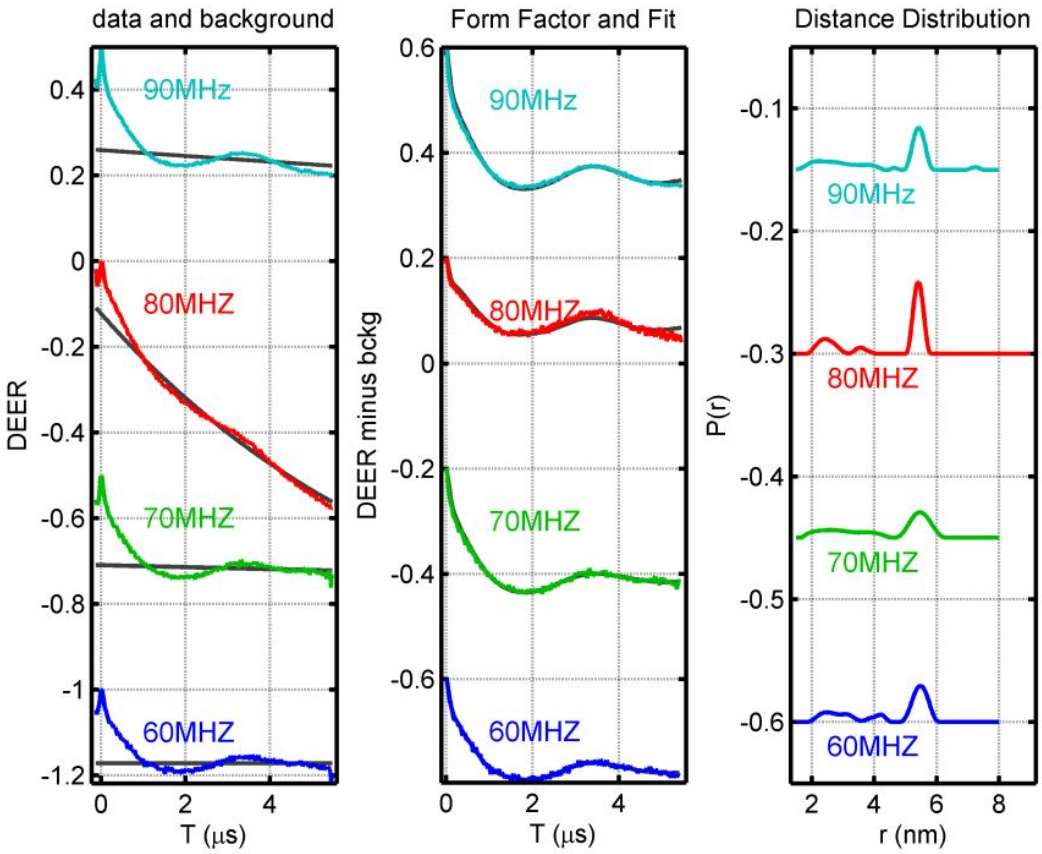

Figure S8: A series of orientation selection experiments for camphor-free BSL-AC at different intervals (90, 80, 70 and 60 MHz) of the probe and pump frequency.

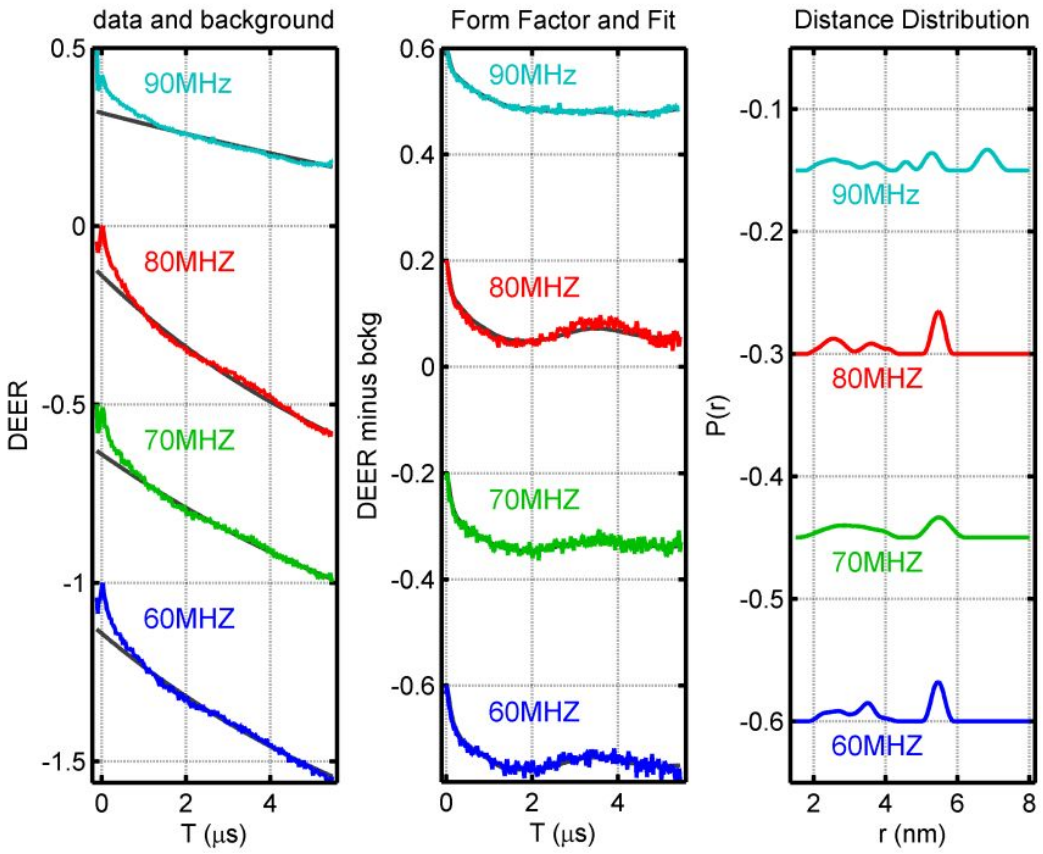

Figure S9: A series of orientation selection experiments for camphor and Pdx bound BSL-AC at different intervals (90, 80, 70 and 60 MHz) of the probe and pump frequency. Notably, the 90 MHz DEER experiment was unsuccessful due to weak echo intensity.

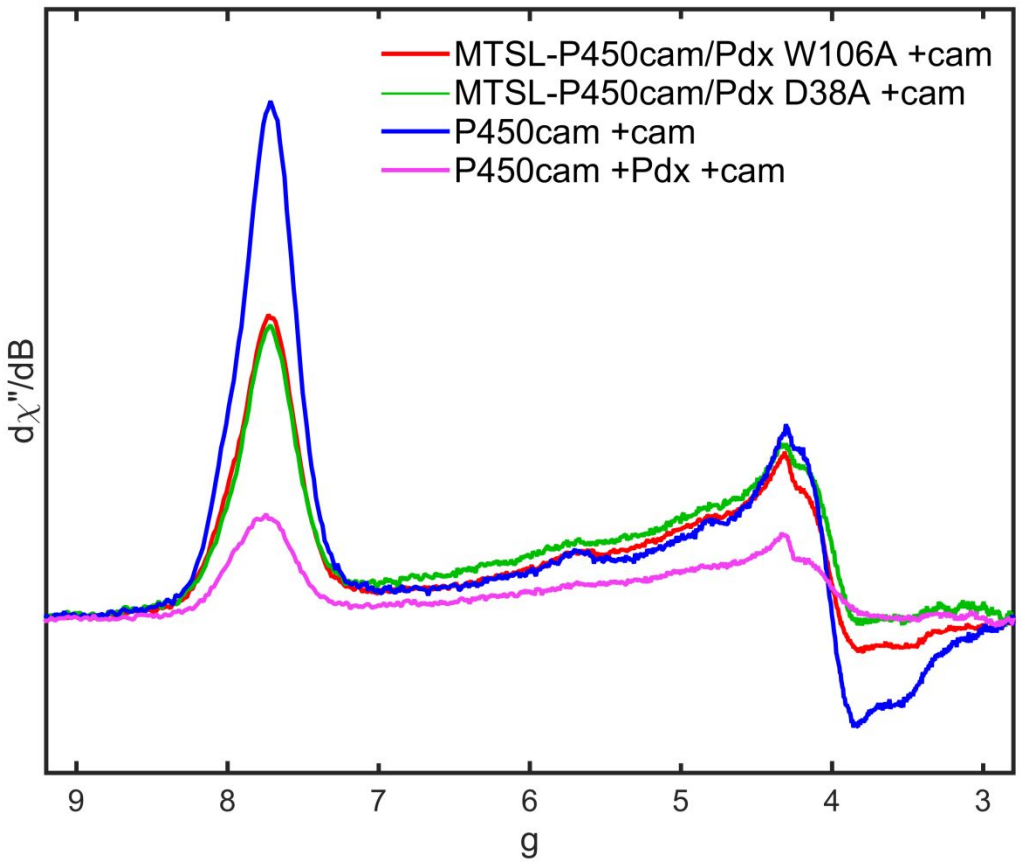

Figure S10 CW EPR spectra of high-spin camphor-bound P450cam in different states and with different Pdx mutants. Shown in blue is the camphor-bound wild type P450cam, and in green and red are the MTSL-FG P450cam with Pdx_{W106A} and Pdx_{D38A}, respectively. The magenta spectrum is the camphor- and Pdx-bound wild type P450cam.

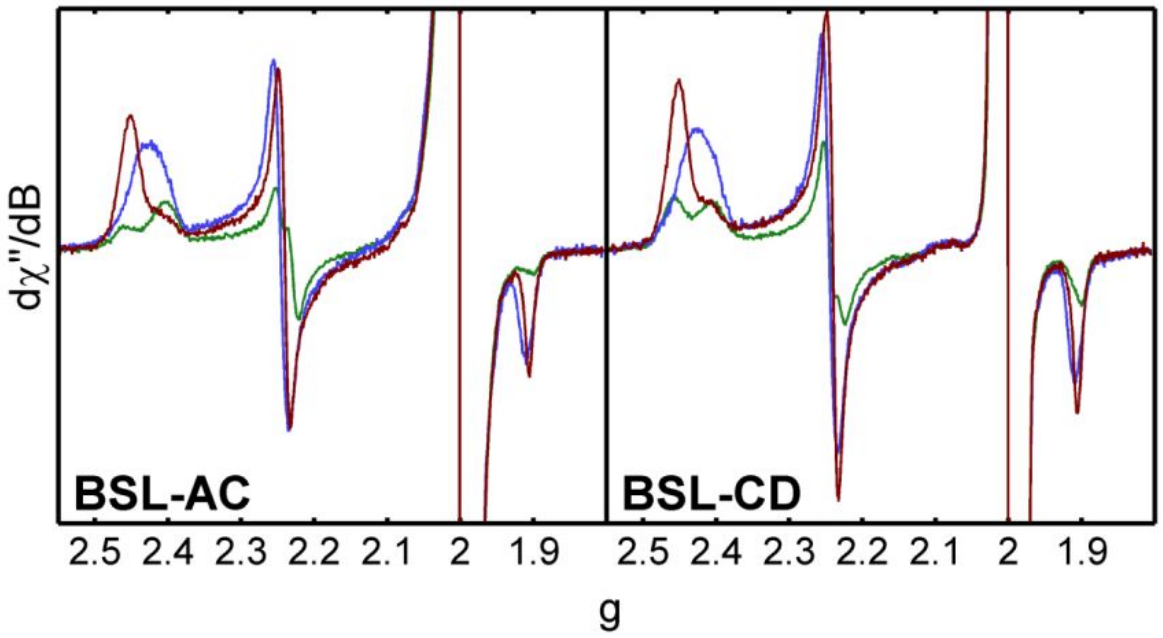

Figure S11. CW EPR spectra of the low-spin signal for BSL-AC (left) and BSL-CD (right). Green and blue curves are camphor-bound and camphor-free P450cam, and the brown curves are the camphor- and Pdx-bound P450cam.

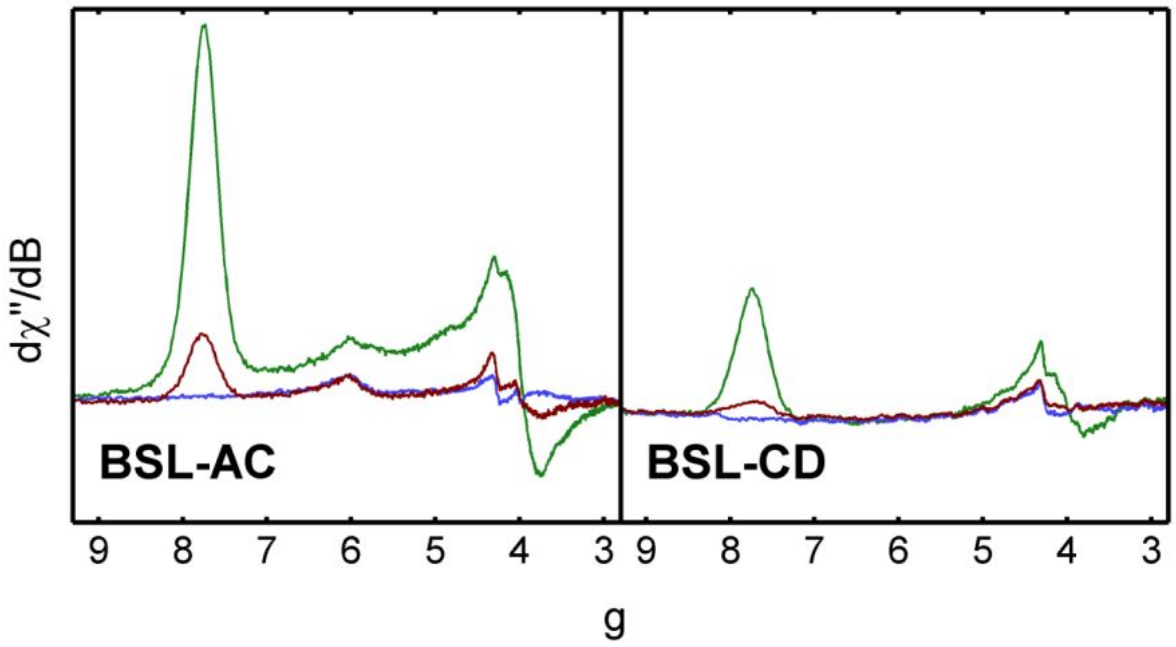

Figure S12. CW EPR spectra of the high-spin signal for BSL-AC (left) and BSL-CD (right). The color schemes are identical to Figure S11.

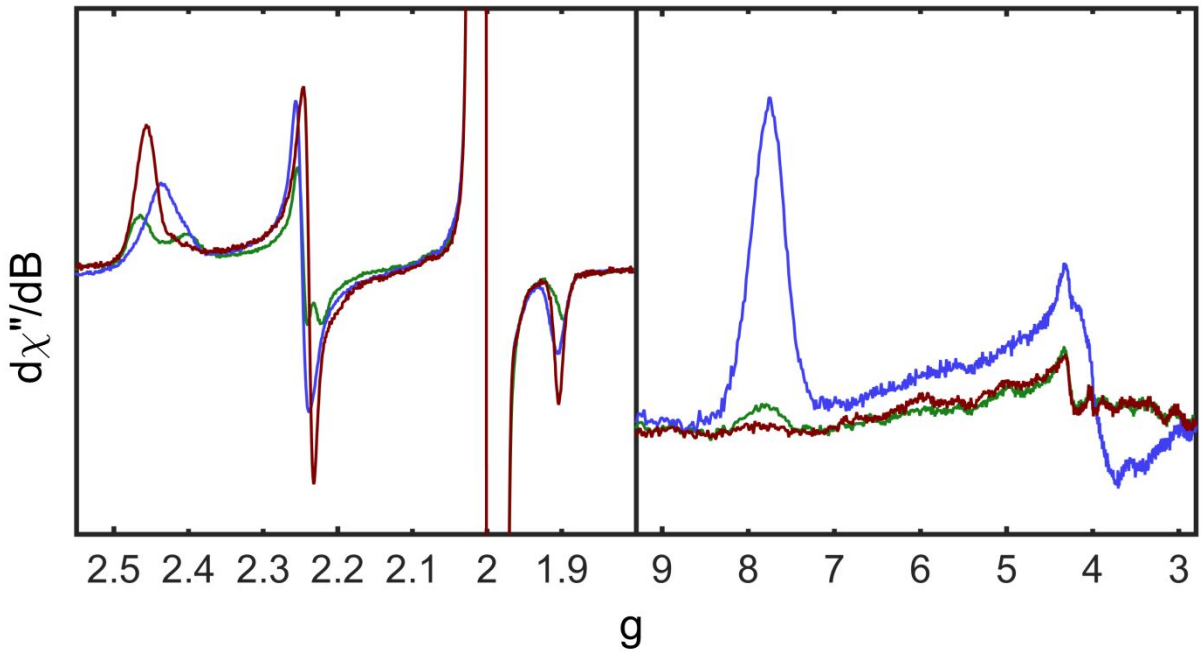

Figure S13. CW EPR spectra of the low-spin (left) and high-spin (right) signal for BSL-AJ. The color schemes are identical to Figure S11.

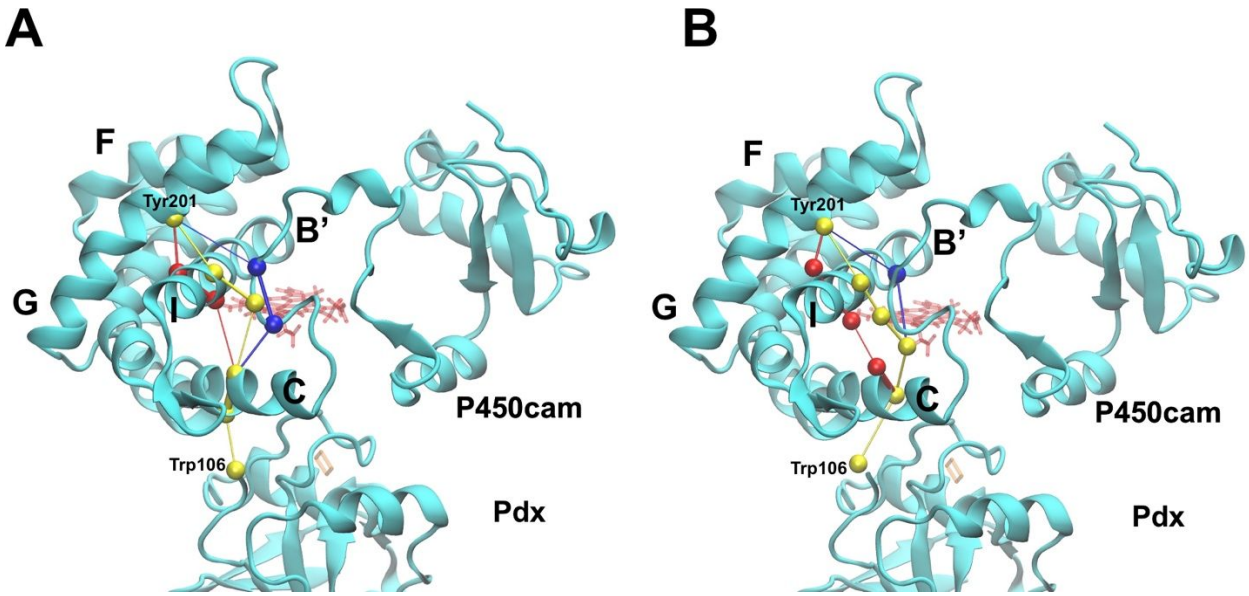

Figure S14. Comparison of dynamic network analysis on the wild-type camphor-bound P450cam-Pdx complex with different node selections. (A) Cα atoms are selected as nodes. (B) Cß atoms are selected as nodes. The camphor-bound P450cam-Pdx complex is shown as a cartoon representation in cyan, and the first three most optimal paths between Tyr201 on P450cam and Trp106 on Pdx are shown in blue, yellow, and red. Two cofactors (heme and iron-sulfur cluster) are shown as red and orange sticks, respectively.

Molecular dynamics simulations

To parameterize BSL, the molecular structure of BSL was obtained from the Protein Data Bank (PDB, PDB ID: 3L2X).[1] The BSL was connected to two cysteine residues, in which ACE and NME were used to cap the N-terminus and C-terminus of each cysteine, and geometry optimization and electrostatic potential calculations were performed in Gaussian09[2] using the Hartree-Fock method[3] with the 6-31G* basis set,[4] and the Antechamber package[5] was used for RESP charge fitting,[6] and Amber preparation files and force field parameters were generated with GAFF.[7] The heme and Fe_2-S_2 cluster parameters were built using MCPB.py module[8] in AmberTools,[9] and parameters for camphor were generated using the GAFF force field[7] with the BCC charge fitting.[10, 11]

The initial coordinates for classical MD simulations of P450cam systems were obtained from the PDB: ferric closed P450cam (P450cam+cam, PDB ID: 2CPP),[12] ferric open P450cam (P450cam, PDB ID: 4JX1, with Pdx, camphor, and hydroxycamphor removed),[13] and ferric open P450cam-Pdx complex (P450cam+cam+Pdx, PDB ID: 4JX1, with camphor removed, and hydroxycamphor replaced with camphor).[13] All crystallographic water molecules were retained, and the systems were built with the LEaP module of AmberTools[9] and were solvated with truncated octahedra of TIP3P water[14] with minimum 10.0 Å cushion. K^+ or Cl^- counterions were used to neutralize the system. All molecular dynamics simulations were performed using AMBER16 with ff14SB force field.[15] Steepest-descent energy minimization was performed for 10000 steps with 100 kcal/mol/Å^2 harmonic restraints first on the entire protein, then on backbone atoms, and followed by another energy minimization without restraints to minimize the entire system. The temperature of the system was gradually increased to 300K in the canonical (NVT) ensemble. For wild-type systems, the equilibration was continued for 7 ns with gradually released harmonic restraints on protein backbone in the isothermal-isobaric (NPT) ensemble, and production runs were conducted for 100 ns in the NPT ensemble (1atm and 300K) without harmonic restraints. For BSL-systems, energy minimization and annealing procedures are the same as described above. The equilibrium was continued for 7 ns with gradually released harmonic restraints on protein backbone in the NPT ensemble, and distance restraints were assigned to maintain the distance between nitroxide nitrogens as the DEER observed distance. Production runs were performed for 100 ns in the NPT ensemble (1atm and 300K) with distance restraints, followed by a gradual restraint release for 7 ns and another 100 ns production run without restraints in the NPT ensemble.

Principal Component Analysis (PCA)

PCA was applied to MD trajectories to extract the essential dynamics of the P450cam-Pdx complex system. In PCA, diagonalization of the covariance matrix of the protein Cα atoms generates a set of eigenvectors and eigenvalues, which describe the correlated motion throughout the protein, and the largest amplitude motion of the protein corresponds to the first principal component (PC1).[16] Before PCA analysis, the solvent, ions, and cofactors were stripped from MD

trajectories using CPPTRAJ module[17] in Amber16, and these MD trajectories were aligned on residues 295-405 of P450cam, where these residues are the structurally invariant core. ProDy interface of Normal Mode Wizard (NMWiz) plugin[18] in Visual Molecular Dynamics (VMD)[19] was used to perform PCA for all backbone of the P450cam-Pdx complex, and the largest principal component was visualized by NMWiz in VMD.

(1) Fleissner, M. R., Bridges, M. D., Brooks, E. K., Cascio, D., Kálai, T., Hideg, K., and Hubbell, W. L. (2011) Structure and dynamics of a conformationally constrained nitroxide side chain and applications in EPR spectroscopy, *Proceedings of the National Academy of Sciences 108*, 16241.

(2) Frisch, M. J., Trucks, G. W., Schlegel, H. B., Scuseria, G. E., Robb, M. A., Cheeseman, J. R., Scalmani, G., Barone, V., Petersson, G. A., Nakatsuji, H., Li, X., Caricato, M., Marenich, A. V., Bloino, J., Janesko, B. G., Gomperts, R., Mennucci, B., Hratchian, H. P., Ortiz, J. V., Izmaylov, A. F., Sonnenberg, J. L., Williams, Ding, F., Lipparini, F., Egidi, F., Goings, J., Peng, B., Petrone, A., Henderson, T., Ranasinghe, D., Zakrzewski, V. G., Gao, J., Rega, N., Zheng, G., Liang, W., Hada, M., Ehara, M., Toyota, K., Fukuda, R., Hasegawa, J., Ishida, M., Nakajima, T., Honda, Y., Kitao, O., Nakai, H., Vreven, T., Throssell, K., Montgomery Jr., J. A., Peralta, J. E., Ogliaro, F., Bearpark, M. J., Heyd, J. J., Brothers, E. N., Kudin, K. N., Staroverov, V. N., Keith, T. A., Kobayashi, R., Normand, J., Raghavachari, K., Rendell, A. P., Burant, J. C., Iyengar, S. S., Tomasi, J., Cossi, M., Millam, J. M., Klene, M., Adamo, C., Cammi, R., Ochterski, J. W., Martin, R. L., Morokuma, K., Farkas, O., Foresman, J. B., and Fox, D. J. (2016) Gaussian 09, Gaussian, Inc., Wallingford CT.

(3) Fock, V. (1930) Näherungsmethode zur Lösung des quantenmechanischen Mehrkörperproblems, *Zeitschrift für Physik 61*, 126-148.

(4) Davidson, E. R., and Feller, D. (1986) Basis set selection for molecular calculations, *Chem. Rev. 86*, 681-696.

(5) Wang, J., Wang, W., Kollman, P. A., and Case, D. A. (2006) Automatic atom type and bond type perception in molecular mechanical calculations, *J. Mol. Graphics Modell. 25*, 247-260.

(6) Bayly, C. I., Cieplak, P., Cornell, W., and Kollman, P. A. (1993) A well-behaved electrostatic potential based method using charge restraints for deriving atomic charges: the RESP model, *J. Phys. Chem. 97*, 10269-10280.

(7) Wang, J., Wolf, R. M., Caldwell, J. W., Kollman, P. A., and Case, D. A. (2004) Development and testing of a general amber force field, *J. Comput. Chem. 25*, 1157-1174.

(8) Li, P., and Merz, K. M. (2016) MCPB.py: A Python Based Metal Center Parameter Builder, *J. Chem. Inf. Model. 56*, 599-604.

(9) D.A. Case, R. M. B., D.S. Cerutti, T.E. Cheatham, III, T.A. Darden, R.E. Duke, T.J. Giese, H. Gohlke, A.W. Goetz, N. Homeyer, S. Izadi, P. Janowski, J. Kaus, A. Kovalenko, T.S. Lee, S. LeGrand, P. Li, C. Lin, T. Luchko, R. Luo, B. Madej, D. Mermelstein, K.M. Merz, G. Monard, H. Nguyen, H.T. Nguyen, I. Omelyan, A. Onufriev, D.R. Roe, A. Roitberg, C. Sagui, C.L. Simmerling, W.M. Botello-Smith, J. Swails, R.C. Walker, J. Wang, R.M. Wolf, X. Wu, L. Xiao and P.A. Kollman. (2016) AMBER 2016, University of California, San Francisco.

(10) Jakalian, A., Jack, D. B., and Bayly, C. I. (2002) Fast, efficient generation of high-quality atomic charges. AM1-BCC model: II. Parameterization and validation, *J. Comput. Chem. 23*, 1623-1641.

(11) Jakalian, A., Bush, B. L., Jack, D. B., and Bayly, C. I. (2000) Fast, efficient generation of high-quality atomic charges. AM1-BCC model: I. Method, *J. Comput. Chem. 21*, 132-146.

(12) Poulos, T. L., Finzel, B. C., and Howard, A. J. (1987) High-resolution crystal structure of cytochrome P450cam, *J. Mol. Biol. 195*, 687-700.

(13) Tripathi, S., Li, H., and Poulos, T. L. (2013) Structural basis for effector control and redox partner recognition in cytochrome P450, *Science 340*, 1227-1230.

(14) Jorgensen, W. L., Chandrasekhar, J., Madura, J. D., Impey, R. W., and Klein, M. L. (1983) Comparison of simple potential functions for simulating liquid water, *The Journal of Chemical Physics 79*, 926-935.
(15) Maier, J. A., Martinez, C., Kasavajhala, K., Wickstrom, L., Hauser, K. E., and Simmerling, C. (2015) ff14SB: Improving the Accuracy of Protein Side Chain and Backbone Parameters from ff99SB, *J. Chem. Theory Comput. 11*, 3696-3713.
(16) Amadei, A., Linssen, A. B. M., and Berendsen, H. J. C. (1993) Essential dynamics of proteins, *Proteins: Structure, Function, and Bioinformatics 17*, 412-425.
(17) Roe, D. R., and Cheatham, T. E. (2013) PTRAJ and CPPTRAJ: Software for Processing and Analysis of Molecular Dynamics Trajectory Data, *J. Chem. Theory Comput. 9*, 3084-3095.
(18) Bakan, A., Meireles, L. M., and Bahar, I. (2011) ProDy: Protein Dynamics Inferred from Theory and Experiments, *Bioinformatics 27*, 1575-1577.
(19) Humphrey, W., Dalke, A., and Schulten, K. (1996) VMD: Visual molecular dynamics, *J. Mol. Graphics 14*, 33-38.